Research Article

Effect of heat treatment on the temperature dependent wear characteristics of electroless Ni–P–BN(h) composite coatings

K. Uday Venkat Kiran[1] · Abhishek Arora[1] · B. Ratna Sunil[2] · Ravikumar Dumpala[1]

Abstract

Nickel–phosphorus composite coatings embedded with boron nitride (BN(h)) particles were deposited on AISI 1018 steel using electroless deposition technique. Then the coatings were heat-treated at 400 °C with an aim to study the role of heat treatment on the temperature-dependent tribological characteristics. The wear characteristics of the as-deposited (AD) and heat-treated (HT) coatings were analyzed at ambient as well as at 300 °C temperature. The surface topography of the wear tracks was studied by using a scanning electron microscope. The hardness of AD samples was measured as increased up to 40% after the high-temperature sliding test due to the semi-coherent Ni_3P phase. High wear resistance was observed in the case of HT coating tested at ambient temperature, which is attributed to the higher hardness and lower amount of adhesive wear during sliding. Furthermore, the effect of heat treatment on the wear rate of the coatings at 300 °C was found to be insignificant.

Keywords Electroless · Boron nitride · Heat treatment · High-temperature wear

1 Introduction

Nickel phosphorous (Ni–P) coatings are adopted in a broad range of industrial applications due to their superior wear resistance and inertness in the corrosion environment [1]. Ni–P coatings show remarkable potential in the oil and gas industry protecting HSLA steels due to excellent corrosion resistance in H_2S and CO_2 environments [2]. Further, the Ni–P coatings show potential in modern machinery in chemical plants and marine applications involving wear and corrosion simultaneously [3, 4]. Ni–P coatings are commonly produced by the chemical reduction of metal ions via a reducing agent [5]. The commonly used electroless baths depending on reducing agents are sodium hypophosphite, amino boranes, sodium borohydride, and hydrazine baths. Sodium hypophosphite baths are most widely (almost 70%) used for depositing Ni–P coatings owing to their higher deposition rates, easy bath control,

and increased stability. Further, for depositing Ni–P alloy coatings acid and alkaline baths are used. The better quality thick coatings are deposited on metals and bath stability is maintained for a long time by employing acid baths. The phosphorus content in the deposits can be easily controlled by varying the pH of hot acid bath (low (3–5% P), medium (6–9% P), and high (10–14% P) phosphorus Ni–P coatings). Warm hypophosphite alkaline baths are employed for depositing Ni–P coatings on plastics and non-metals [6]. Embedding nano or sub-micron particles into the Ni–P matrix to acquire functional properties to the coated surfaces has been well demonstrated in the literature [6, 7].

Nickel-based coatings are suitable for elevated temperature tribological applications as they possess a high melting point (1480 °C) and good oxidation resistance. Self-lubricating coatings perform relatively better in a few specific applications where dry sliding conditions are

demanded at elevated temperatures due to the working environment. If the friction coefficient is more at the elevated temperatures, the performance and life of the surface coatings are severely affected. In order to address these issues, integrating appropriate solid lubricant particles into the Ni–P coatings has been reported as a promising strategy [8]. Several researcher articles have reported co~deposition of solid lubricant particles such as MoS_2, PTFE, BN(h), WS_2, Ag, carbon nanotubes, and graphite into Ni–P matrix in order to enhance the tribological characteristics of the coating [9–13].

Lower shear strength along the sliding direction, optimum mechanical strength, high temperature stability, oxidation, and corrosion resistance are the essential attributes required for a self-lubricating composite coating targeted for high-temperature tribological applications [14]. Boron nitride, BN(h), exhibits high thermal and chemical stability along with a high melting point (~ 2973 °C) which make BN(h) a potential material to incorporate in Ni–P matrix to improve the temperature effected tribological behavior. Similar to graphite, BN(h) exhibits a layered structure that exhibits a strong covalent bond inside the layer and weak van der Waals forces among layers [15]. Researchers explored oxidation, wear, and corrosion behavior of Ni–P–BN(h) coatings considering the significance of the coatings in industrial applications [16–18]. Self-lubrication and anti-frictional properties make the coating one of a potential candidate for wide-spread tribological applications. Some specific applications include components for dry lubrication (pistons), tooling molds for excellent release properties, and flat sliding joints in machine tools for low coefficient of friction. Bello et al. successfully synthesized Ni–P coated BN(h) using electroless deposition technique, thus enhancing the potential of the material for tribological applications [19]. Leon et al. [20] investigated the tribological characteristics of heat-treated Ni–P–BN(h) composite coatings against alumina ball at high temperatures. The results revealed that the friction coefficient and wear increases with the increase in test temperature. The wear mechanism was observed as transformed at elevated temperatures from mild adhesive wear to combination of adhesive and fatigue wear when the temperature was reduced to at ambient temperature.

Several authors reported considerable enhancement in the wear characteristics of the Ni–P composite coatings by implementing a suitable heat treatment cycle [3, 21, 22]. Jiang et al. [23] and Sivandipoor et al [24] observed that the heat treatment of Ni–P coatings incorporated with solid lubricant particles has improved the tribological characteristics. Baibordi et al. [25] showed the enhanced hardness and wear resistance in duplex Ni–P/Ni–B–BN composite coatings upon heat-treatment at 400 °C attributed to crystalline nature and Ni_3B phase precipitation.

From the works of Leon et al.[26], it can be understood that the wear coefficient of heat-treated Ni–P–BN(h) composite coating has been decreased up to two orders of magnitude compared with conventional Ni–P coating at ambient temperature conditions. It can be learned from the available literature, that the wear characteristics of Ni–P composite coatings at ambient temperature sliding conditions can be improved by adopting an appropriate heat treatment process. However, information on the role of heat treatment on the performance of Ni–P–BN(h) coatings at high temperature sliding wear conditions is insufficient. In the current work, the role of heat-treatment on the temperature dependent tribological characteristics of BN(h) incorporated Ni–P-composite coatings has been investigated with an aim to understand the wear mechanisms.

2 Experimental methods and materials

2.1 Ni–P–BN(h) composite coatings deposition

BN(h) reinforced Ni–P composite coatings were deposited on AISI 1018 grade steel substrate of dimensions 20 mm × 20 mm × 5 mm using electroless plating technique. Substrate preparation and electroless nickel plating details were discussed elsewhere [27]. The proprietary electroless Ni–P solution comprising of 5–6 g/l nickel (as a sulfate solution), 27–33 g/l sodium hypophosphite (NaH_2PO_2), suitable amounts of stabilizer and complexant was utilized for depositing Ni–P–BN(h) coatings. As a standard practice, to avoid structural defects and to get better coating substrate adhesion, initially for 30 min, Ni–P coating was developed, and then a BN(h) incorporated Ni–P composite coating was deposited for 2 h 30 min as per the following procedure. In the first step, before adding BN(h) into the electrolyte, BN(h) suspension was dispersed in 10 ml of electrolyte for 1 h under ultrasonic agitation. Then, BN(h) was co-deposited into the Ni–P metal matrix by adding ultrasonicated suspension of BN(h) particles in the electrolyte under continuous magnetic stirring at 350 rpm to avoid agglomeration of particles. Table 1 shows the operating parameters for the deposition of electroless Ni–P–BN(h) coatings.

Based on the available literature, the heat-treatment of Ni–P coatings at 400 °C resulted in tremendous improvement of hardness and wear resistance of coatings attributed to the transition from amorphous to crystalline nature and precipitation of Ni_3P phase during heat-treatment. Several researchers highlighted the importance of heat-treatment (particularly 400 °C) in Ni–P composite coating systems for improving wear resistance [21, 28]. Industrially, 400 °C for 1 h heat-treatment cycle is commonly

Table 1 Operating parameters for deposition of Ni–P–BN(h) composite coating

Deposition parameters	Ni–P/hBN coating
Nickel metal	5–6 g L^{-1}
Sodium hypophosphite	27–33 g L^{-1}
pH	5.7–6.3
Temperature	87 ± 2 °C
Stirring mechanism	Magnetic stirring (350 rpm)
BN dispersion	5% by volume
Deposition time	3 h
Bath volume	150 ml

implemented for widespread applications to achieve peak hardness. By considering all these aspects, in the present study, heat treatment of as-deposited Ni–P–BN(h) samples was carried out at 400 °C for 1 h and further annealed in the furnace.

2.2 Characterization

The phase structure of the BN(h) particles, and Ni–P–BN(h) composite coatings was evaluated using X-ray diffractometer (Bruker XRD, D8 advanced) using CuKα (λ = 1.5405 Å) as a source of radiation in the 2θ ranges from 20° to 80°. Surface topography, cross-sectional, and wear track analysis of the deposited coatings were carried out using scanning electron microscope (JEOL JSM-638OA) attached with energy dispersive X-ray spectroscopy (EDS) for carrying out elemental analysis. The microhardness of the coatings was evaluated using Vickers hardness tester by applying 100 g load for 15 s (Mitutoyo, HM-112).

The friction and wear behaviour of the Ni–P–BN(h) coatings was evaluated using reciprocating friction tester (DUCOM India, TR-281). Sliding tests of the coatings were conducted against AISI E52100 steel ball of 6 mm diameter at ambient temperature and also at high temperature (300 °C) for 100 m sliding distance. The normal load of 10 N was applied with 10 mm stroke length and a frequency of 3 Hz. Following the wear tests, weight loss was measured using a weighing balance of 0.1 mg accuracy, and the specific wear rate was calculated using the following Eq. (1).

$$Specific\ wear\ rate = \frac{wear\ volume}{(normal\ load \times sliding\ distance)} \quad (1)$$

Wear test samples were designated as ADRT and HTRT for as-deposited coatings and heat-treated coatings for room temperature (RT) tests, and AD300 and HT300 for as-deposited coatings and heat-treated coatings for tests conducted at 300 °C, respectively.

3 Results and discussion

3.1 Structural analysis of BN(h) particles

SEM and XRD analysis of BN(h) particles are presented in Figs. 1 and 2, respectively. From the SEM micrograph (Fig. 1), the morphology of BN(h) powder was observed as flake-like morphology with particle size ranging from 1 to 3 μm. Figure 1a, b depicts the BN(h) particles are agglomerated and comprises of irregular plate-like crystals. From the XRD analysis (Fig. 2), sharp and distinct peaks corresponding to hexagonal boron nitride. The peak at 26.6° in the XRD pattern has been assigned to the (002) reflection of the graphite-like BN(h) structure [29]. The atomic plane of crystal BN(h) consists of hexagonal rings formed with B and N atoms possessing the strong covalent bond between them and separated by the weak van der Waals bonding between the atomic planes, thereby offering lubricating properties [30].

3.2 Surface morphology of Ni–P–BN(h) deposits

Figure 3 shows the surface morphology of AD and HT Ni–P–BN(h) coatings. The formation of smooth, defect-free, and nodular structure is attributed to the uniform, steady-state reduction and adsorption of nickel ions on the substrate due to the optimal concentration of reducing agent in the electrolyte. The average size and bubble-like features increased in the heat-treated coating (Fig. 3b) which is attributed to the evolution of entrapped hydrogen gas from the coating during heat treatment.

Cross-sectional SEM image of Ni–P–BN(h) coating (Fig. 4a), clearly demonstrates the defect-free interfacial integrity of the coating and substrate. Initially, 10–12 μm thickness (30 min) conventional nickel phosphorous (Ni–P) coating was grown on the substrate followed by Ni–P–BN(h) deposition for the next 48 μm (150 min), as seen in the magnified BSE cross-sectional view (Fig. 4b) of the coating. Figure 4a, b shows the uniform distribution of BN(h) particles in the Ni–P matrix. Further, Fig. 4c shows the magnified back-scattered electron (BSE) image of the polished sample showing the distribution of BN(h) particles. Spot EDS analysis (Fig. 4d) confirms the presence of all constituent elements, nickel, phosphorus, boron, and nitrogen.

3.3 Phase analysis of Ni–P–BN(h) deposits

Figure 5 presents the XRD results of AD and HT Ni–P–BN(h) coatings. XRD patterns of the Ni–P–BN(h) coatings revealed that the incorporation of BN(h) particles into the
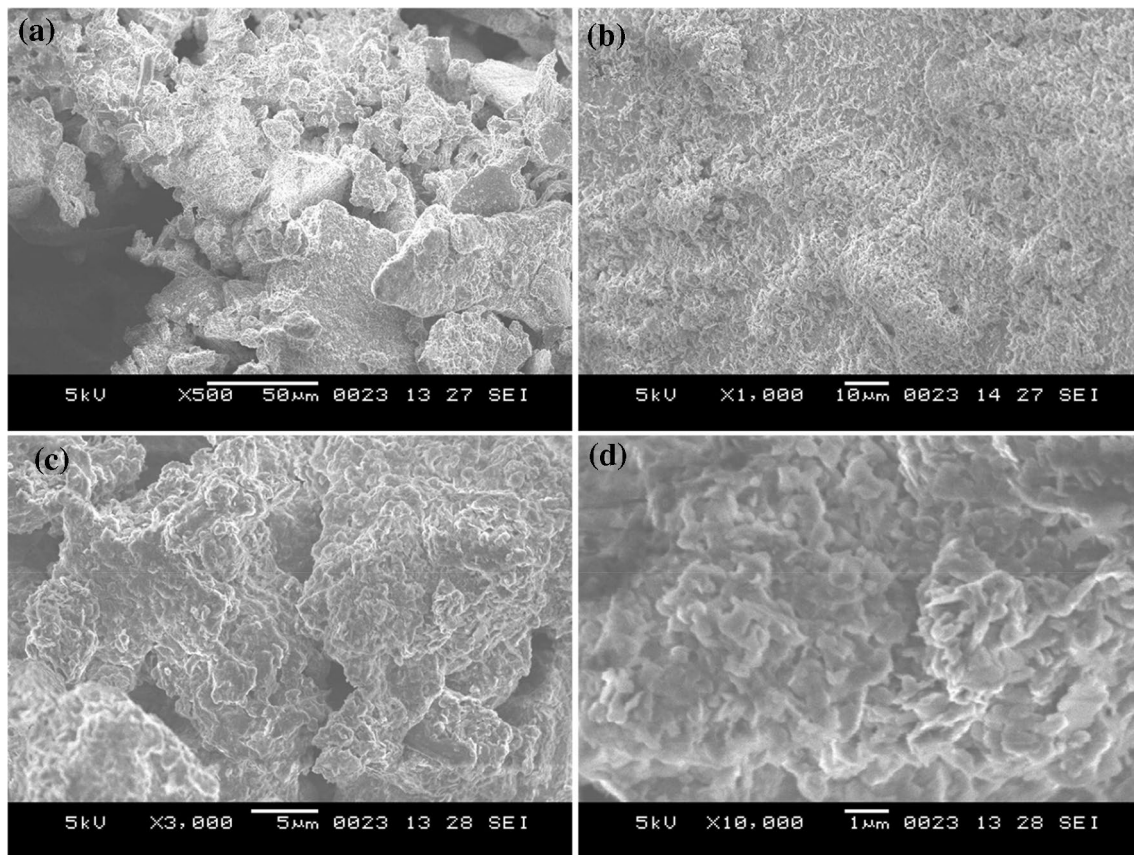
Fig. 1 Surface morphology of BN(h) particles at different magnifications **a** 500×, **b** 1000×, **c** 3000×, and **d** 10,000×
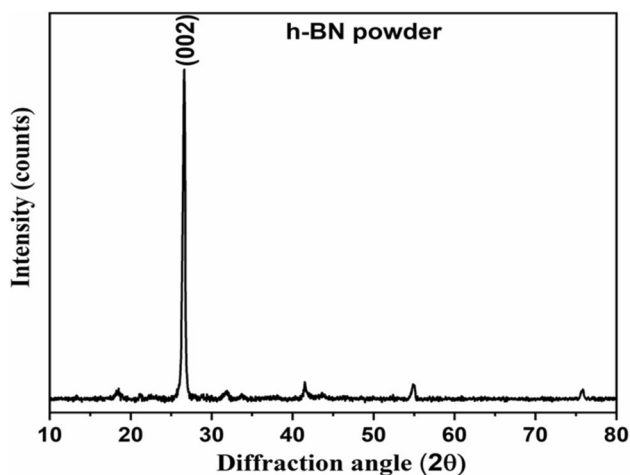

Fig. 2 X-ray diffraction pattern of BN(h) particles

Ni–P matrix did not affect the crystal structure of the coatings [31]. BN(h) characteristic peak is not observed in the XRD patterns, due to the lower volume content of BN(h) particles and high structure factor of nickel. The broad peak observed in the XRD pattern of AD coating at 44.5°

corresponds to (111) diffraction peak of FCC nickel. XRD peak broadening is usually appeared due to fine crystallite size and/or micro-strain present in deposits [32]. XRD pattern of HT coating (at 400 °C) shows two phases, i.e., Ni and Ni_3P. Higher intensity narrow width peaks indicate the more degree of crystallinity and large crystallite size of the HT coatings.

3.4 Microhardness

Microhardness of AD and HT coatings were measured as 383 ± 18 $HV_{0.1}$ and 720 ± 12 $HV_{0.1}$, respectively (Fig. 6). The reinforcement of BN(h) particles into the coating have not shown any significant effect on the hardness, which can be attributed to the relative softness of the BN(h) particles. The hardness of as-deposited Ni–P–BN(h) coating is dependent on the BN(h) particles and phosphorus content in the coating. Hsu et al. [33] reported the hardness of Ni–P–BN(h) coating decreases with an increase in BN(h) content from 8.61 to 11.74 vol.%, whereas above 11.74% the hardness increases attributed to variation in the phosphorus content in the coating. The hardness of as-deposited Ni–P–BN(h) reported at optimum BN(h)
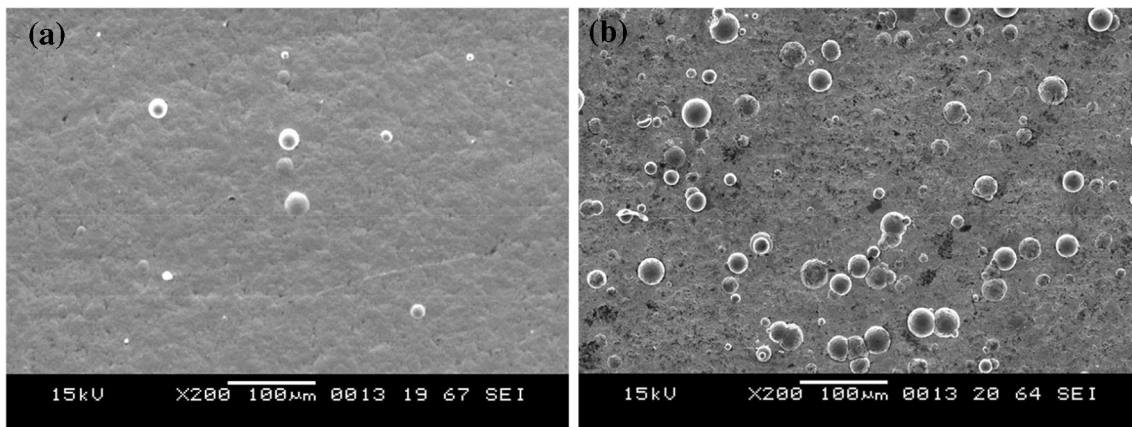
Fig. 3 Surface morphology of Ni–P–BN(h), **a** as-deposited, and **b** heat-treated coatings
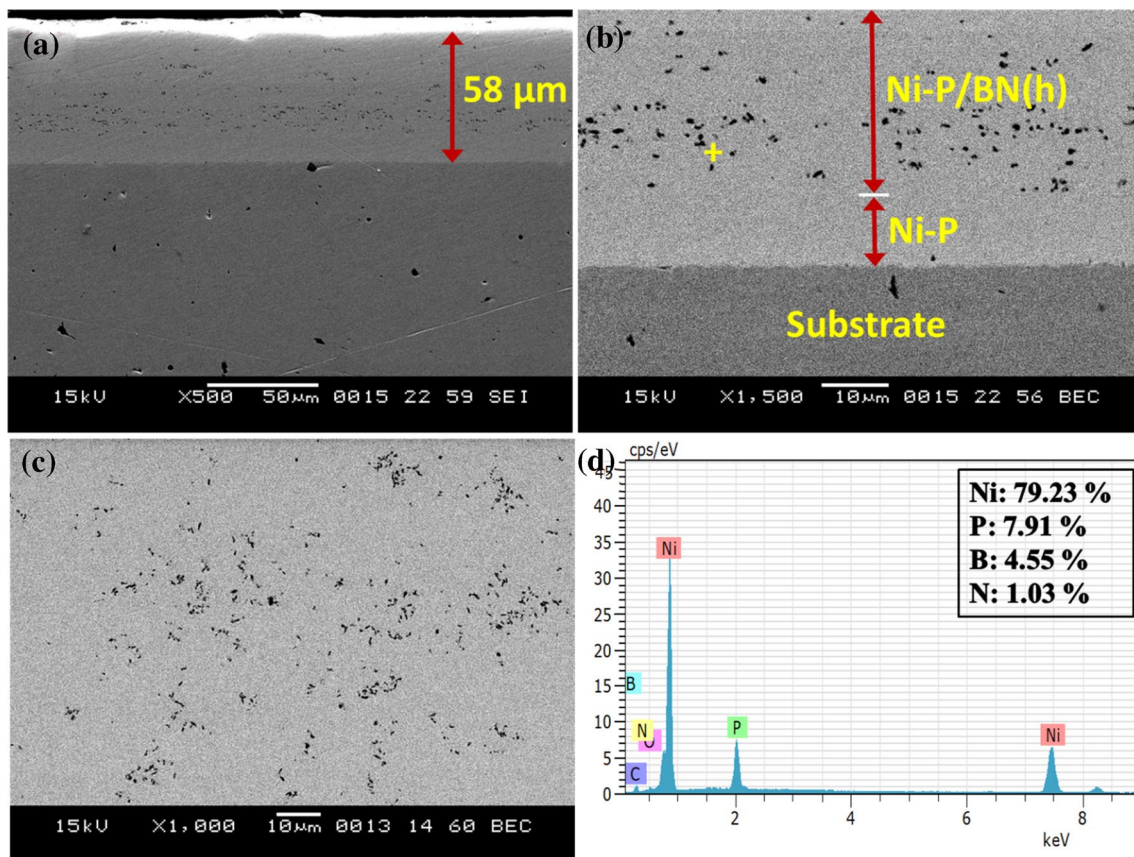

Fig. 4 SEM images of Ni–P–BN(h) composite coatings, **a** SE image and, **b** BSE image, showing the cross-section and **c** polished sample showing the distribution of BN(h) particles. **d** Spot EDS analysis (in **b**, plus symbol)

concentration is 442 HV. Ni$_3$P phases were formed during the heat treatment (confirmed from XRD analysis) is found to be responsible for increased hardness for HT Ni–P–BN(h) coating. Several authors reported that the peak hardening effect in Ni–P composite coatings is achieved at 400 °C ascribed to the crystallization of Ni and precipitation of Ni$_3$P phase [34–36]. As known, the hardness is a measure of material local resistance against plastic deformation. The Ni$_3$P phase precipitated during heat treatment, acts as a barrier for dislocation motion, thus resulting in restrained plastic deformation, thereby resulting in enhanced hardness.
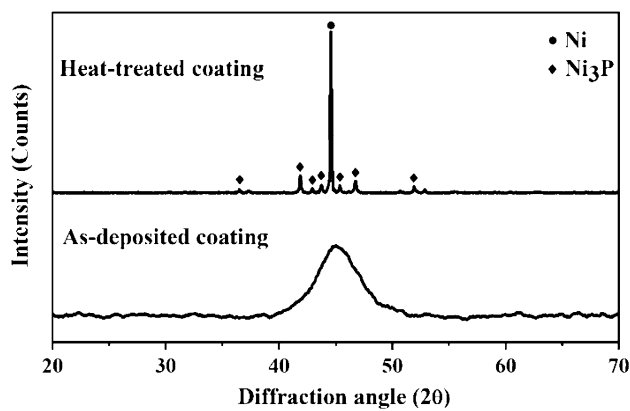
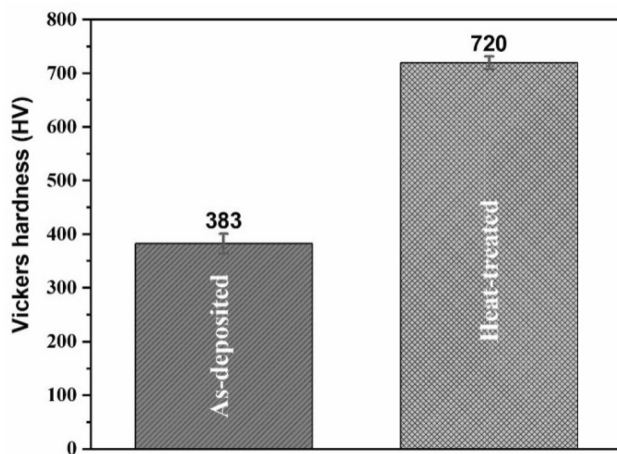**Fig. 5** XRD patterns of as-deposited and heat-treated Ni–P–BN(h) coatings

Fig. 6 Vickers micro-hardness of Ni–P–BN(h) as-deposited and heat-treated coatings

3.5 Friction curves and wear characteristics

Figure 7 compares the variation in friction coefficient for AD and HT Ni–P–BN(h) composite coatings at ambient temperature and 300 °C. AD coating presents two friction stages at ambient temperature sliding conditions. In the first stage, a low and stable friction coefficient (from ~ 0.25 to 50 m sliding distance) is observed, which is attributed to the coating lubricity obtained by incorporating BN(h) particles. In the second stage, i.e., after 50 m, a sudden rise in friction coefficient value was observed which is attributed to the increased contact area between the coating and steel ball during sliding. The friction coefficient value of the HT coating has been observed to be stable compared to AD coating over the entire sliding duration; attributed to the low contact area between coating and steel ball tested under the same loading conditions. Similar kind of
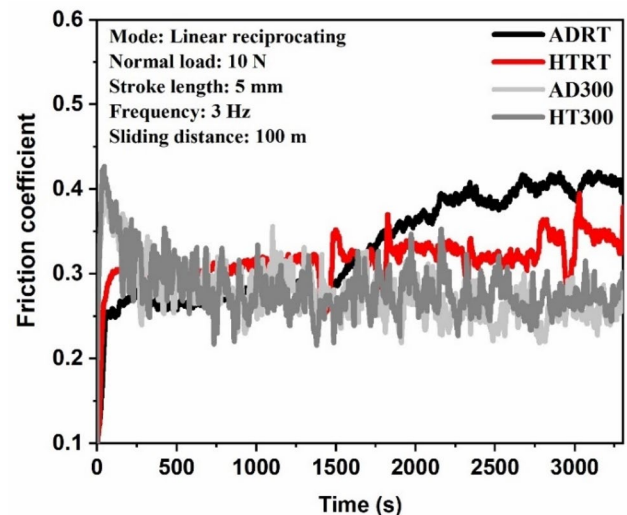

Fig. 7 Frictional characteristics of as-deposited and heat-treated Ni–P–BN(h) coatings tested at ambient and 300 °C temperatures

performance was also reported for Ni–P–BN(h) coating heat-treated at 400 °C, Ni–P–WS$_2$ coating, and Ni–P-PTFE autocatalytic coatings [24, 26]. Goettems et al. [37] investigated the tribological characteristics of Ni–P coatings with hard-chromium coatings using a ball and flat configuration tribometer. Friction coefficient values reported at the end of wear tests for as-deposited, heat-treated (at 400 °C) Ni–P coatings and hard chromium coating are 0.8, 0.55, and 0.6, respectively. The friction coefficient observed at the end of wear tests for AD, and HT Ni–P–BN(h) coatings are 0.4 and 0.3, respectively, which are considerably below the reported values. Friction coefficient values of AD and HT coatings at 300 °C were observed to fluctuate between 0.21–0.35 over the entire sliding distance. This phenomenon of friction coefficient fluctuations can be understood by considering the intermittent formation and infringement of the tribo-chemical layer at the contact surface. Mukhopadhyay et al. observed similar behavior i.e., higher instability in friction coefficient of Ni–P–Mo coating at 300 °C sliding conditions attributed to continuous formation and breakage of tribo-oxide layer [38].

Figure 8 represents the wear rate of AD and HT Ni–P–BN(h) coatings at the ambient temperature and 300 °C. At ambient temperature, wear rate of the HT coating (4.49×10^{-5} m^3/N-m) was observed as lower (3 orders of magnitude) compared with the as-deposited coating (1.45×10^{-4} m^3/N-m). This behavior can be attributed to the effect of higher hardness and enhanced shear strength in HT coatings. Leon et al. demonstrated similar kind of behavior for Ni–P–BN(h) composite coatings that are heat-treated at 400 °C due to Ni$_3$P phase precipitation [26]. Sribalaji et al. reported the enhanced shear strength in the heat-treated Ni–P coating attributed to the
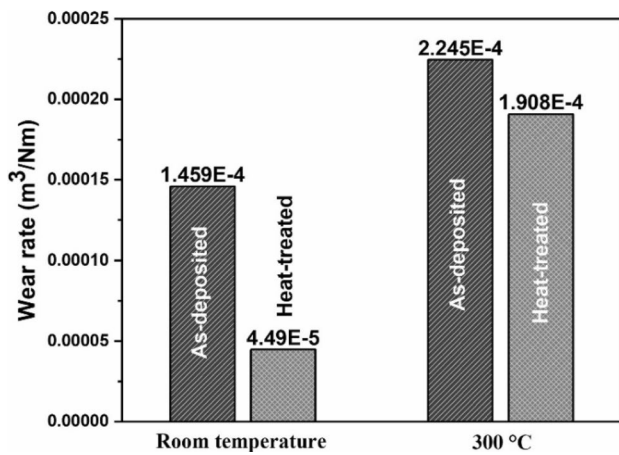
Fig. 8 Wear rate of as-deposited and heat-treated Ni–P–BN(h) coatings at ambient temperature and 300 °C

hindrance of dislocation motion by the Ni_3P precipitate subsequently resulted in high scratch resistance [32]. At 300 °C, wear rate of AD and HT coatings were measured as

2.24×10^{-4} m³/N-m and 1.90×10^{-4} m³/N-m, respectively. The higher wear rate observed for Ni–P–BN(h) coatings at 300 °C compared to ambient temperature, which is attributed to the malleable and ductile nature of the coatings at high temperature, irrespective of the coating condition. On the other hand, the variation in the wear rate was not significant for AD and HT coatings tested at 300 °C due to in-situ temperature-induced Ni_3P phase formation in AD coatings. This is similar to the findings of Franco et al. [39], due to slight crystalline nature resulted from in-situ heat treatment while conducting the wear experiments.

3.6 Wear mechanisms

Figure 9 shows the wear track (conducted at the ambient temperature) image and elemental analysis of AD Ni–P–BN(h) coating. The sliding track width of AD coating is measured as 428 µm, as shown in the SEM image (Fig. 9a). The magnified view of wear track (Fig. 9b) revealed the shearing of as-deposited coating along with the sliding direction under the continuous action
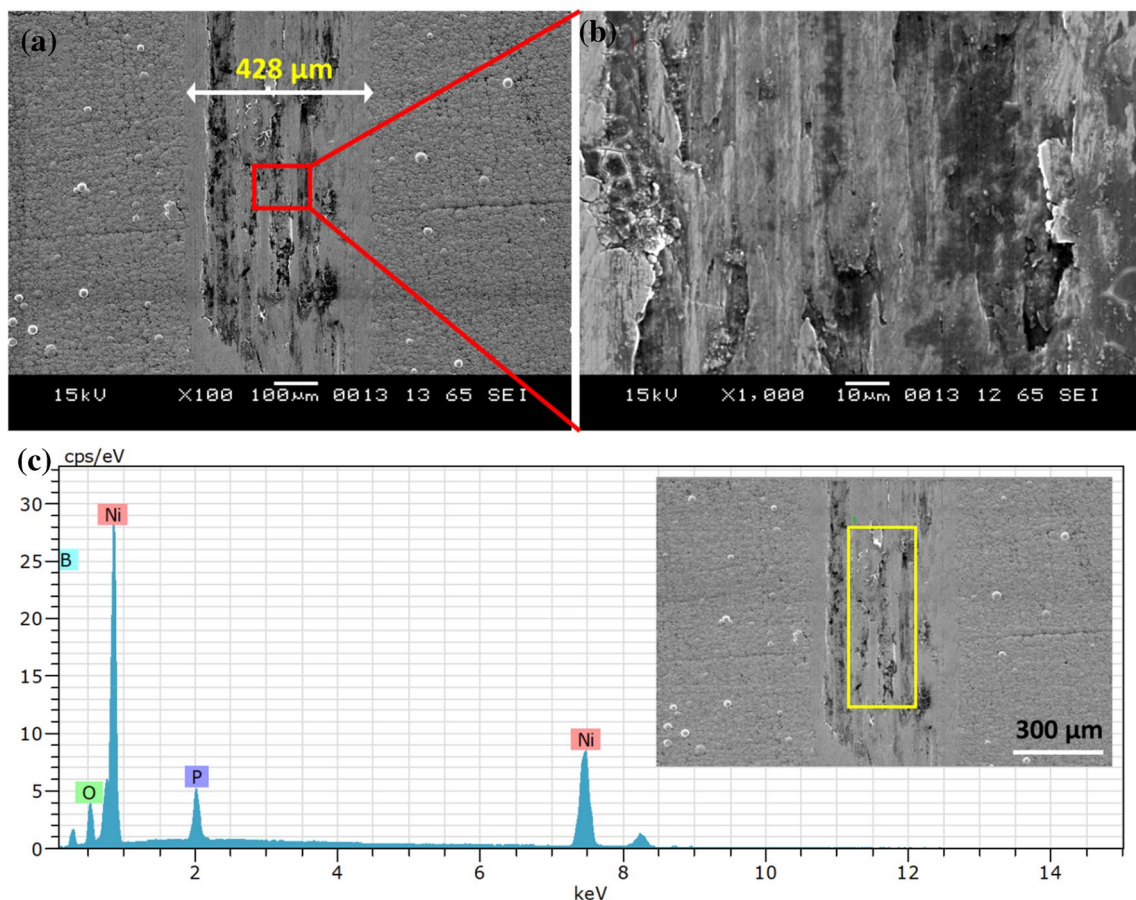

Fig. 9 Wear analysis of as-deposited coating at ambient temperature **a** SEM image showing sliding track width, **b** enlarged view, and **c** elemental analysis of the marked region

of cyclic loading. During reciprocating sliding under normal load, sub-surface layers are subjected to cyclic shear stresses and results in micro-crack formation. Coating ductility and mutual solubility between the AD coating and steel ball contribute to material transfer and resulted in layered wear track morphology. The adhesion is attributed to the ductile nature of the coating and low sliding speed, resulting in the formation of temporary adhesion bonds under high stress sliding test conditions. If the surfaces are separated by any barrier such as oxide layer or surfaces possess lower solubility, the obtained adhesion bond strength is usually observed as lower for the contacting pairs. Therefore, tearing arises at the interface, and a minimum material loss appears. However, in the present work, the surface coating acts as soft material compared with the AISI E52100 steel ball and the tearing happens inside the softer material. Then a fraction of coating material is drawn towards the AISI E52100 steel ball and deformed under the continuous sliding conditions. Furthermore, the presence of oxygen (5.30 wt%) along with Ni and P from the elemental

analysis on the wear track of AD coating (Fig. 9c) confirms the occurrence of triboxidation.

Figure 10 shows the sliding track width and elemental analysis of HT Ni–P–BN(h) coating at ambient temperature sliding conditions. The width of the wear track on HT coating (172 µm) has been measured as lower compared with the wear track on AD coating (428 µm) suggests the higher load-bearing capacity of AD coating. Figure 10b reveal the smooth wear track with a mild degree of material flow and minimum wear debris. Heat treatment along with BN(h) incorporation reduced the adhesive wear, which can be attributed to the decreased mutual solubility between coating and steel ball. Wear track features at higher magnification revealed no considerable deterioration and/or longitudinal grooves, thus confirming the lower abrasion when sliding against hardened steel ball. Further, elemental analysis of the sliding track (Fig. 10c) confirmed no significant presence of oxygen, thus signifying less oxidative and adhesive wear. Sivandipoor et al. [24], also observed similar kind of wear behavior in the HT Ni–P–WS$_2$ coatings, when sliding against pin made of hardened steel.
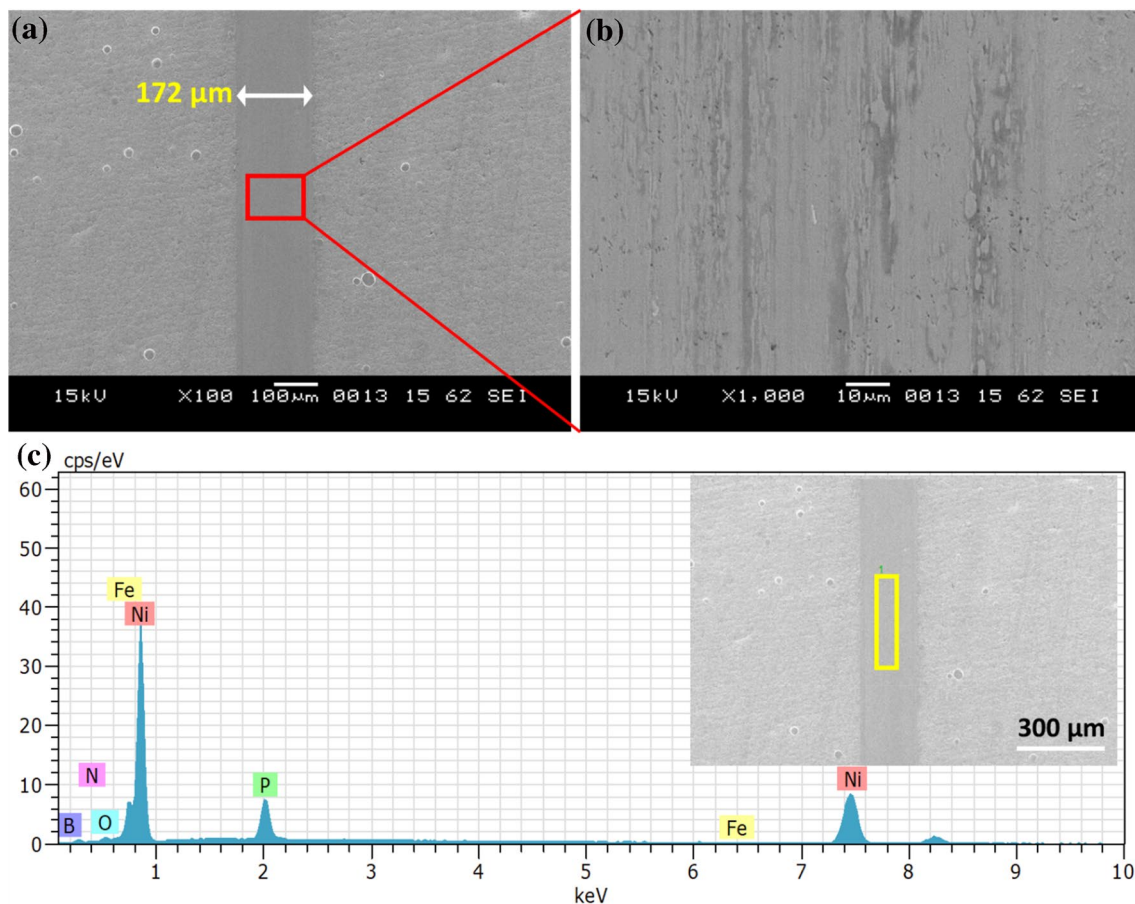

Fig. 10 Sliding track details of HT coating at ambient temperature **a** micrograph showing sliding track width, **b** enlarged view, and **c** elemental analysis of the marked region

Figures 11, 12 show the sliding track morphology and elemental analysis of AD and HT coatings tested at 300 °C. The wear track widths of both AD and HT coatings were measured as similar, i.e., 780 µm and 782 µm, respectively (Figs. 11a, 12a), which is ascribed to the in-situ phase transformations during high-temperature sliding. During high temperature (300 °C) wear test, the as-deposited coatings gained significant hardness, up to 40%, which is attributed to in-situ heat treatment as explained by Kundu et al. [40]. Other studies also demonstrated structural changes in as-deposited coatings when the wear tests were conducted at elevated temperatures [39, 40]. In the present work, wear tracks (Figs. 11b, 12b) shows the formation of linear grooves along the direction of sliding. The ductility of AD and HT Ni–P–BN(h) composite coating at high temperatures is responsible for the higher amount of plastic deformation and formation of more wear debris. Wear debris that is produced during sliding undergoes localized hardening, and tend to entrap between coating and counter-body. The abrasive action of these particles

results in groove formation in the wear track, which is evident from the macrographs of the wear tracks. Deep scratches observed in Fig. 12b indicates the transfer of material from coating to the counter-body during sliding. Elemental analysis of the wear track of AD and HT coatings at 300 °C (Figs. 11c, 12c) revealed no considerable presence of oxygen on the wear track.

Elemental analysis of wear tracks of AD and HT Ni–P–BN(h) coatings at ambient and 300 °C revealed the presence of Ni, P, and O, whereas there was no presence of Fe on the wear track thus confirming that the coating sustained the failure under the test conditions of high contact stresses. Hence, from the results, it can be understood that the combined effect of higher hardness due to Ni_3P phase precipitation and lubricity due to the presence of BN(h) particles resulted in better wear resistance for HT coatings tested at ambient temperature. Whereas, the higher amount of wear rate was observed at high temperature (300 °C) sliding conditions because of the high adhesive wear.
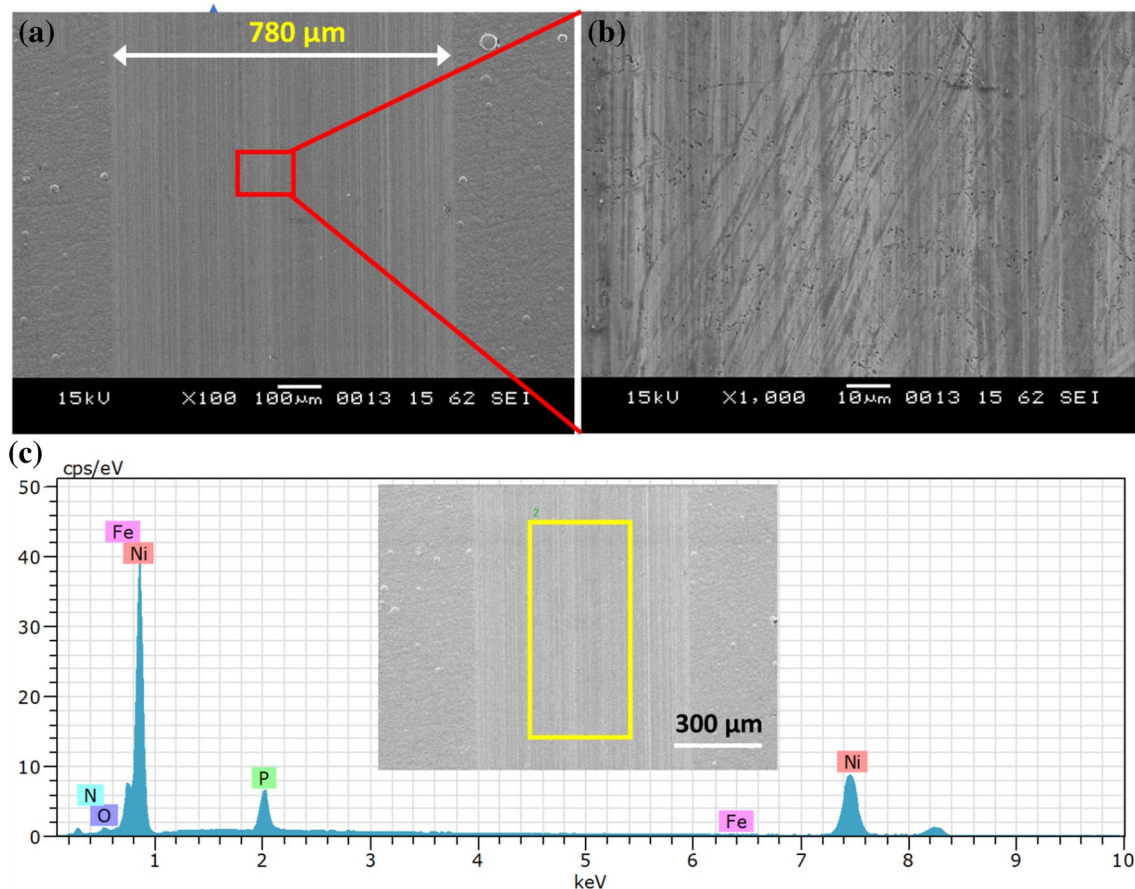

Fig. 11 Sliding track details of AD coating at 300 °C, **a** micrograph showing sliding track width, **b** enlarged view, and **c** elemental analysis of the marked region
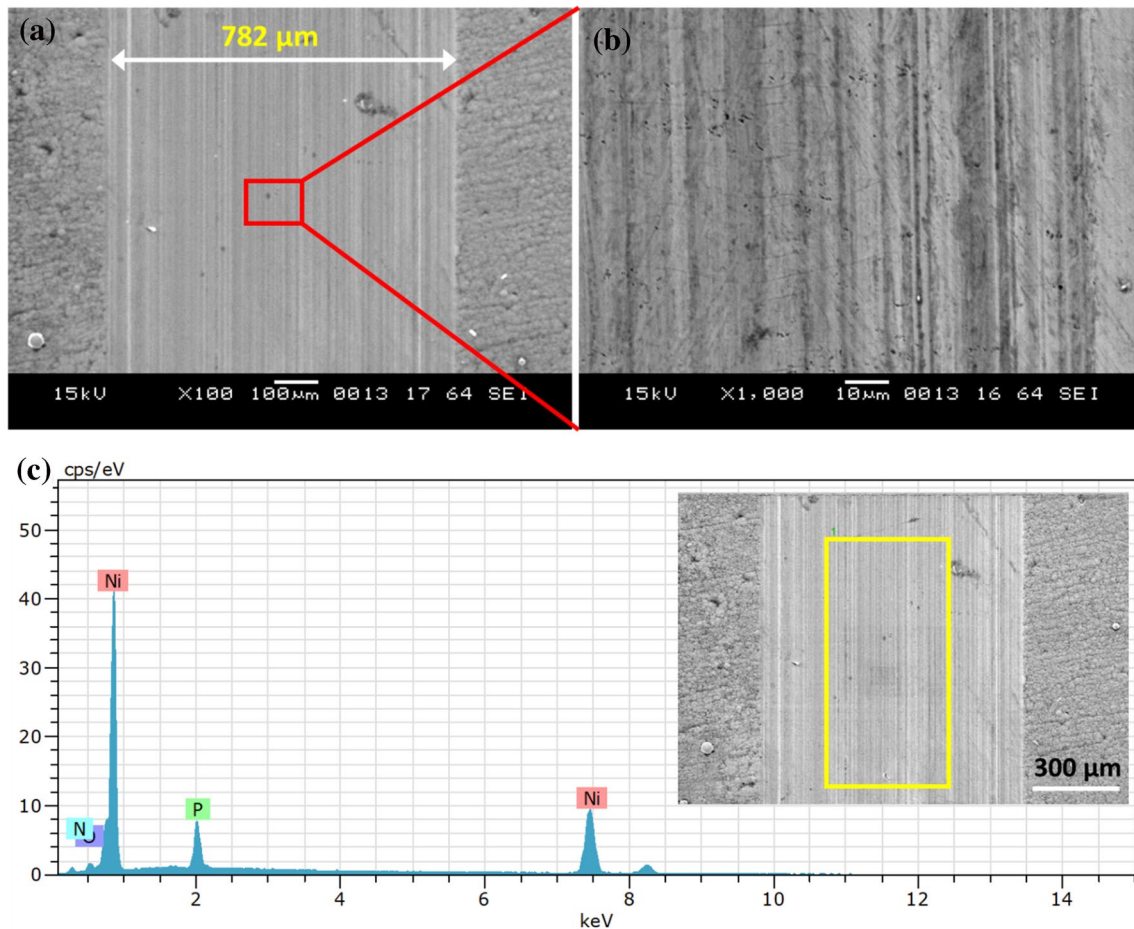
Fig. 12 Sliding track details of HT coating at 300 °C, **a** micrograph showing sliding track width, **b** enlarged view, and **c** elemental analysis of the marked region

4 Conclusions

Nickel phosphorus coatings containing BN(h) solid lubricant particles were successfully deposited on AISI 1018 steel substrate using electroless deposition technique. Heat treatment of Ni–P–BN(h) composite coatings resulted in crystallization of the amorphous Ni phase and precipitation of Ni_3P phase, as confirmed from the XRD analysis. The semi-coherent Ni_3P phase is found to be responsible for the higher hardness of heat-treated coatings (720 ± 12 $HV_{0.1}$), whereas as-deposited coatings exhibited the hardness of 383 ± 18 $HV_{0.1}$. Under ambient temperature sliding conditions, heat-treated coatings exhibited high wear resistance (4.49×10^{-5} m^3/N-m), about 3 orders magnitude in comparison to that of the as-deposited coatings (1.49×10^{-4} m^3/N-m). The better wear performance is attributed to the synergetic effect of self-lubrication and the high hardness of the heat-treated coatings. Whereas, under high temperature (300 °C) sliding conditions, higher wear rates were observed for both the as-deposited

(2.24×10^{-4} m^3/N-m) and heat-treated (1.90×10^{-5} m^3/N-m) coatings. Also, the role of heat treatment on the sliding wear performance of Ni–P–BN(h) coatings is found to be insignificant at high temperature sliding conditions.

Compliance with ethical standards

References

1. Agarwala RC, Agarwala V (2003) Electroless alloy/composite coatings: a review. Sadhana 28(3):475–493. https://doi.org/10.1007/BF02706445

2. Wang C, Farhat Z, Jarjoura G, Hassan MK, Abdullah AM (2017) Indentation and erosion behavior of electroless Ni–P coating on pipeline steel. Wear 376:1630–1639

3. Sahoo P, Das SK (2011) Tribology of electroless nickel coatings—a review. Mater Des 32(4):1760–1775. https://doi.org/10.1016/j.matdes.2010.11.013

4. Wang J, Yan F, Xue Q (2009) Friction and wear behavior of ultra-high molecular weight polyethylene sliding against GCr15 steel and electroless Ni–P alloy coating under the lubrication of seawater. Tribol Lett 35(2):85–95

5. Mallory GO, Hajdu JB (1990) Electroless plating: fundamentals and applications. Cambridge University Press, Cambridge

6. Sudagar J, Lian J, Sha W (2013) Electroless nickel, alloy, composite and nano coatings—a critical review. J Alloy Compd 571:183–204. https://doi.org/10.1016/j.jallcom.2013.03.107

7. Pancrecious JK, Ulaeto SB, Ramya R, Rajan T, Pai B (2018) Metallic composite coatings by electroless technique—a critical review. Int Mater Rev 63(8):488–512

8. Sharma A, Singh AK (2013) Electroless Ni–P and Ni–P–Al$_2$O$_3$ nanocomposite coatings and their corrosion and wear resistance. J Mater Eng Perform 22(1):176–183. https://doi.org/10.1007/s11665-012-0224-1

9. Hu X, Jiang P, Wan J, Xu Y, Sun X (2009) Study of corrosion and friction reduction of electroless Ni–P coating with molybdenum disulfide nanoparticles. J Coat Technol Res 6(2):275–281. https://doi.org/10.1007/s11998-008-9131-7

10. Alirezaei S, Monirvaghefi SM, Saatchi A, Ürgen M, Motallebzadeh A (2013) High temperature tribology of nanocrystalline Ni–P–Ag coating. Surf Eng 29(4):306–311. https://doi.org/10.1179/1743294412Y.0000000085

11. Chen WX, Tu JP, Xu Z, Tenne R, Rosensteig R, Chen WL, Gan HY (2002) Wear and friction of Ni-P electroless composite coating including inorganic fullerene-WS$_2$ nanoparticles. Adv Eng Mater 4(9):686–690

12. Wu Y, Shen B, Liu L, Hu W (2006) The tribological behaviour of electroless Ni–P–Gr–SiC composite. Wear 261(2):201–207

13. Sharma A, Singh AK (2014) Electroless Ni–P–PTFE-Al$_2$O$_3$ dispersion nanocomposite coating for corrosion and wear resistance. J Mater Eng Perform 23(1):142–151. https://doi.org/10.1007/s11665-013-0710-0

14. Torres H, Rodríguez Ripoll M, Prakash B (2018) Tribological behaviour of self-lubricating materials at high temperatures. Int Mater Rev 63(5):309–340. https://doi.org/10.1080/09506608.2017.1410944

15. Eichler J, Lesniak C (2008) Boron nitride (BN) and BN composites for high-temperature applications. J Eur Ceram Soc 28(5):1105–1109. https://doi.org/10.1016/j.jeurceramsoc.2007.09.005

16. Ranganatha S, Venkatesha T (2017) Fabrication and anticorrosion performance of Ni–P–BN nanocomposite coatings on mild steel. Surf Eng Appl Electrochem 53(5):449–455

17. Farrokhzad M (2017) High temperature oxidation behaviour of autocatalytic Ni–P–BN (h) coatings. Surf Coat Technol 309:390–400

18. Leon O, Staia M, Hintermann H (2005) Wear mechanism of Ni–P–BN (h) composite autocatalytic coatings. Surf Coat Technol 200(5–6):1825–1829

19. Bello K, Maleque M, Ahmad Z (2015) Synthesis and characterization of Ni–P coated hexagonal boron nitride by electroless nickel deposition. Surf Eng Appl Electrochem 51(6):523–529

20. León OA, Staia MH, Hintermann HE (2003) High temperature wear of an electroless Ni–P–BN (h) composite coating. Surf Coat Technol 163–164:578–584. https://doi.org/10.1016/S0257-8972(02)00663-1

21. León-Patiño CA, García-Guerra J, Aguilar-Reyes EA (2019) Tribological characterization of heat-treated Ni–P and Ni–P–Al$_2$O$_3$

22. composite coatings by reciprocating sliding tests. Wear 426–427:330–340. https://doi.org/10.1016/j.wear.2019.02.015

23. Mohammadi M, Ghorbani M (2011) Wear and corrosion properties of electroless nickel composite coatings with PTFE and/or MoS$_2$ particles. J Coat Technol Res 8(4):527–533. https://doi.org/10.1007/s11998-011-9329-y

24. Jiang J, Chen H, Zhu L, Qian W, Han S, Lin H, Wu H (2016) Effect of heat treatment on structures and mechanical properties of electroless Ni–P–GO composite coatings. RSC Adv 6(110):109001–109008. https://doi.org/10.1039/C6RA22330C

24. Sivandipoor I, Ashrafizadeh F (2012) Synthesis and tribological behaviour of electroless Ni–P–WS2 composite coatings. Appl Surf Sci 263:314–319. https://doi.org/10.1016/j.apsusc.2012.09.051

25. Baibordi A, Amini K, Bina M, Dehghan A (2014) The effect of heat treatment temperature on the properties of the composite duplex electroless coating of Ni–P/Ni–B–BN containing boron nitride nanoparticles. Kovové Materiály 52(5):263–268

26. León OA, Staia MH, Hintermann HE (1999) Influence of the heat treatment on the tribological behavior of a Ni–P–BN(h) autocatalytic composite coating. Surf Coat Technol 120–121:641–645. https://doi.org/10.1016/S0257-8972(99)00438-7

27. Uday Venkat Kiran K, Arora A, Sunil BR, Dumpala R (2018) Sliding wear characteristics of as-deposited and heat-treated electroless Ni–P coatings against AISI E52100 steel ball. Mater Res Exp 6(3):036401. https://doi.org/10.1088/2053-1591/aaf2f9

28. Chockalingam S, Natarajan U, Selvam M, Cyril AG (2016) Investigation on machinability and damping properties of nickel-phosphorus coated boring bar. Arab J Sci Eng 41(2):669–676

29. Matović B, Luković J, Nikolić M, Babić B, Stanković N, Jokić B, Jelenković B (2016) Synthesis and characterization of nanocrystaline hexagonal boron nitride powders: XRD and luminescence properties. Ceram Int 42(15):16655–16658. https://doi.org/10.1016/j.ceramint.2016.07.096

30. Podgornik B, Kosec T, Kocijan A, Donik Č (2015) Tribological behaviour and lubrication performance of hexagonal boron nitride (h-BN) as a replacement for graphite in aluminium forming. Tribol Int 81:267–275

31. Balaraju JN, Sankara Narayanan TSN, Seshadri SK (2003) Electroless Ni–P composite coatings. J Appl Electrochem 33(9):807–816. https://doi.org/10.1023/a:1025572410205

32. Sribalaji M, Arunkumar P, Babu KS, Keshri AK (2015) Crystallization mechanism and corrosion property of electroless nickel phosphorus coating during intermediate temperature oxidation. Appl Surf Sci 355:112–120. https://doi.org/10.1016/j.apsusc.2015.07.061

33. Hsu C-I, Hou K-H, Ger M-D, Wang G-L (2015) The effect of incorporated self-lubricated BN (h) particles on the tribological properties of Ni–P/BN (h) composite coatings. Appl Surf Sci 357:1727–1735

34. Apachitei I, Tichelaar FD, Duszczyk J, Katgerman L (2002) The effect of heat treatment on the structure and abrasive wear resistance of autocatalytic NiP and NiP–SiC coatings. Surf Coat Technol 149(2):263–278. https://doi.org/10.1016/S0257-8972(01)01492-X

35. Palaniappa M, Seshadri SK (2007) Hardness and structural correlation for electroless Ni alloy deposits. J Mater Sci 42(16):6600–6606. https://doi.org/10.1007/s10853-007-1501-5

36. Karthikeyan S, Vijayaraghavan L, Madhavan S, Almeida A (2016) Study on the mechanical properties of heat-treated electroless NiP coatings reinforced with Al$_2$O$_3$ nano particles. Metall Mater Trans A 47(5):2223–2231. https://doi.org/10.1007/s11661-016-3413-y

37. Goettems FS, Ferreira JZ (2017) Wear behaviour of electroless heat treated Ni-P coatings as alternative to electroplated hard chromium deposits. Mater Res 20(5):1300–1308

38. Mukhopadhyay A, Barman TK, Sahoo P (2017) Tribological behavior of sodium borohydride reduced electroless nickel alloy coatings at room and elevated temperatures. Surf Coat Technol 321:464–476

39. Franco M, Sha W, Aldic G, Malinov S, Çimenoğlu H (2016) Effect of reinforcement and heat treatment on elevated temperature sliding of electroless Ni–P/SiC composite coatings. Tribol Int 97:265–271. https://doi.org/10.1016/j.triboint.2016.01.047

40. Kundu S, Das SK, Sahoo P (2019) Friction and wear behavior of electroless Ni–P–W coating exposed to elevated temperature. Surfaces Interfaces 14:192–207. https://doi.org/10.1016/j.surfin.2018.12.007